Solid State Phenomena
ISSN: 1662-9779, Vol. 391, pp 11-20
doi:10.4028/p-wUhTP5

Submitted: 2025-12-05
Revised: 2026-02-26
Accepted: 2026-02-26
Online: 2026-04-20

Modulated Pulsed Electrochemical Machining of Tungsten Carbide-Cobalt: An Experimental Study According to DIN SPEC 91399

Alexander Thielecke[1,a*], Pascal Clauß[1,b], Gunnar Meichsner[1,c], Philipp Damm[1,d], Guido Jungblut[2,e], Marco Schäfer[2,f] Matthias Hackert-Oschätzchen[1,g]

[1]Chair of Manufacturing Technology with Focus Machining, Faculty of Mechanical Engineering, Otto von Guericke University Magdeburg, Universitätsplatz 2, 39106 Magdeburg, Germany

[2]Pro-Com A. Jungblut GmbH, Gewerbegebiet Heiligenwies 17, 66663 Merzig, Germany

[a]alexander.thielecke@ovgu.de, [b]pascal.clauss@ovgu.de, [c]gunnar.meichsner@ovgu.de, [d]philipp.damm@ovgu.de, [e]ajungblut@pro-com-web.de, [f]mschaefer@pro-com-web.de, [g]matthias.hackert-oschaetzchen@ovgu.de (*corresponding author)

Keywords: Modulated Pulsed Electrochemical Machining, Cemented Carbides

Abstract. The following study examines the experimental determination of the electrochemical machinability of cemented carbides with a neutral electrolyte solution. In previous research, a removal mechanism of tungsten carbide-cobalt was demonstrated applying pulsed electrochemical machining. This work focuses on the material removal of tungsten carbide-cobalt with the further developed modulated pulsed electrochemical machining process according to DIN SPEC 91399. Compared to the preceding investigation, the modulated pulsed technique demonstrates a similar removal mechanism with higher current efficiencies.

Introduction

Cemented carbides. Cemented carbides are composite materials containing a hard material phase (e. g. tungsten carbide - WC) embedded in a metallic binder matrix (e. g. cobalt - Co), which leads to excellent mechanical properties [1]. On the other hand, its mechanical properties make WC-Co to a difficult-to-cut material [2]. Therefore, electrochemical machining (ECM) is chosen as an alternative machining process, since ECM is capable of machining metals regardless of their mechanical properties like hardness and toughness [3]. The current state of the art is that WC-Co is electrochemically machined with modified, highly corrosive electrolytes [4, 5, 6]. If the pH ranges at which dissolution of tungsten and cobalt is thermodynamically possible are plotted on a pH scale, there is no overlap – which is displayed in Fig. 1 [7].

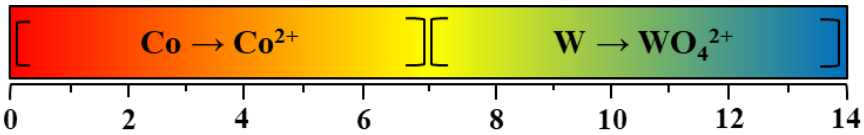

Fig. 1. Areas of active dissolution of tungsten and cobalt in relation to the pH value of the electrolyte, adapted from [7]

The anodic oxidation reaction of tungsten in acidic and weakly alkaline solutions can be expressed as in Eq. 1 [8]:

$$W + 3H_2O = W0_3 + 6H^+ + 6e^- \quad (1)$$

Accordingly, the tungsten component forms a solid, non-conductive oxide layer (WO_3) when WC-Co is machined with neutral electrolytes such as sodium nitrate solution ($NaNO_3$), which in turn prevents the electrochemical removal process.

Previous experiments. In previous experiments, a removal mechanism of WC-Co with $NaNO_3$ as the electrolyte was demonstrated by applying pulsed electrochemical machining (PECM). In this work, anodic dissolution of cobalt, an oxidation of tungsten followed by a mechanical separation of the tungsten oxide layer, and the separation of tungsten carbide after the dissolution of the cobalt were shown. With suitable parameter sets, material removal was generated at slow feed rates (0.02 mm/min). Nevertheless, permanent material removal could not be maintained because after a certain distance between the electrodes, the working gap became too small due to the formation of the passivating oxide layer, which led to the experiments being terminated [9].

Modulated pulsed electrochemical machining. The modulated pulsed electrochemical machining (MPECM) process is based on the PECM process which is characterised by an oscillating cathode and a pulsed direct current. PECM itself is an advanced machining process based on the ECM sinking process, where the tool is lowered towards the workpiece and transfers its negative shape into the workpiece. PECM is characterized by an oscillating cathode and a pulsed direct current to reduce the working gap to obtain higher accuracy in consequence of a higher localized current density [10]. In MPECM, the cathode is controlled by a programmable linear axis rather than by a mechanical oscillation. This technical feature allows switching several current pulses at the bottom dead center of the cathode. Fig. 2 illustrates this principle.

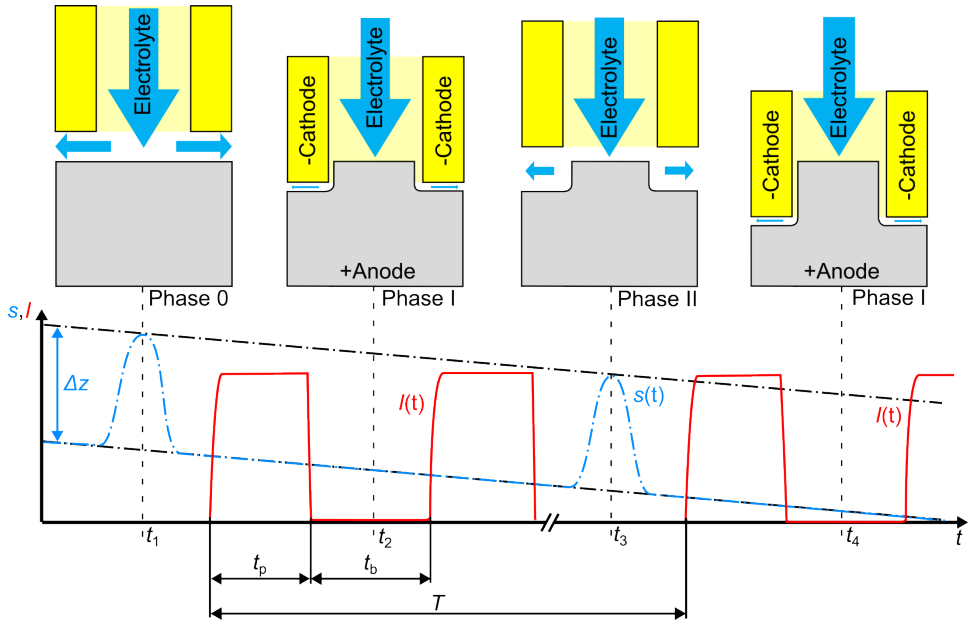

Fig. 2. Principle of MPECM with multiple modulated direct current pulses [11]

The schematic illustration of the MPECM process shown in Fig. 2 is divided into three phases. Phase 0 represents the initial state of the process. In this phase, the anode (workpiece) and cathode (tool electrode) are positioned at the predefined working gap, and no electrochemical machining takes place. In phase I, the machining process (anodic dissolution of the workpiece material) takes place applying a defined number of current pulses. During this phase, the cathode is located at the bottom dead center while maintaining the specified working gap. Phase II describes the flushing phase. No machining current is applied in this phase. The cathode moves to top dead center and the working gap is cleared of reaction products, gas bubbles, and dissolved material. Phases I and II are repeated cyclically until the desired depth of removal is achieved. MPECM therefore enables processing with several short pulses between the flushing phases. Shorter current pulses during machining reduce the working gap and thus also the ohmic resistance. This leads to a reduction in the dispersion of the electric current and an increase in the local current density, which enhances the precision of the machining process. Previous experiments with PECM showed that longer pulses resulted in a less stable removal process with WC-Co. It appears that the longer pulses allow the oxide layer more time to grow, leading to a more homogeneous and thicker oxide layer that interrupts the material removal

process [9]. Accordingly, this study experimentally investigates the material removal of WC-Co applying MPECM. The material-specific removal characteristics, surface appearances and microstructure were evaluated.

Material

The removal experiments were conducted using a commercially available CKi®12 from *Gerhard Ihle Hartmetalle Werkzeuge e.K.*, a tungsten carbide-cobalt type. Images of the base material were taken using a scanning electron microscope (SEM) Hirox SH 5500. Fig. 3 shows the surface of the material.

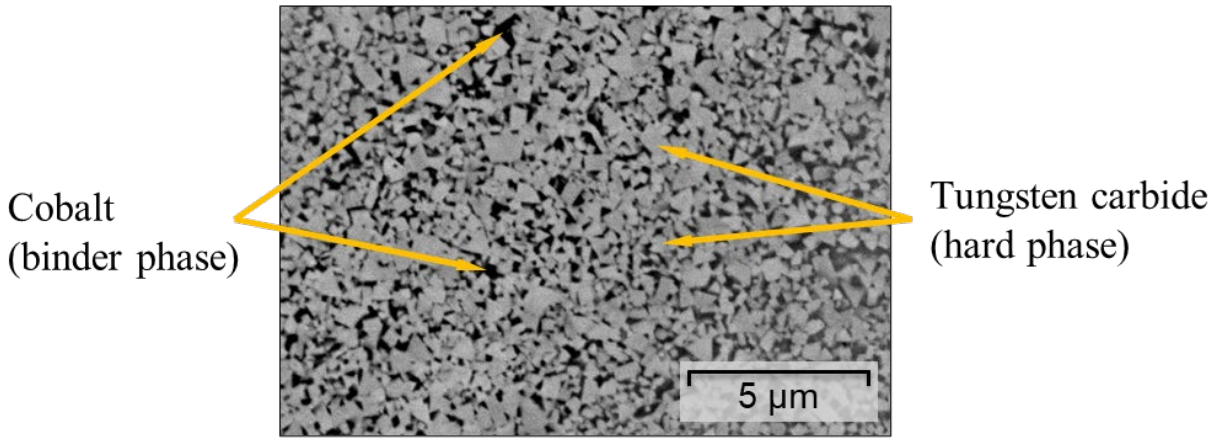

Fig. 3. Material contrast image of a ground, etched sample

The microstructure shows that a large part of the material consists of the hard and wear-resistant WC phase, while the cobalt binder is evenly distributed. The average grain size of the tungsten carbide grains corresponds to the manufacturer's specifications of 0.5 µm. The distribution of the elements was analyzed by applying an energy dispersive X-ray analysis (EDX). The chemical composition is shown in Table 1.

Table 1. Chemical composition of CKi®12

Element		WC	W	C	Co
Manufacturer specification	p_i [%]	88	-	-	12
EDX	p_i [%]	-	76.98	12.40	10.63

The batch of test specimens used corresponds to that in [9].

Design of Experiments

DIN SPEC 91399. To ensure the comparability of the results from the PECM and the MPECM removal experiments, the experiments in this work were carried out according to the DIN SPEC 91399 [9, 12]. The DIN SPEC 91399 specifies a methodology with which process input parameters for PECM processes can be systematically determined. For this analysis, the aim was to obtain the material specific removal characteristic. For this purpose, the removal rate v_a and the current efficiency η as a function of the current density J, as well as the removed mass m_a as a function of the flowed electrical charges Q, were experimentally determined. The analyzed parameters are described in Table 2.

Table 2. Analyzed parameters to describe material-specific removal characteristics

Parameter	Description
Removal rate $v_a(J)$ [mm/min]	Anodic material removal rate as a function of the average current density flowing on the removal surface
Current efficiency η [%]	Proportion of the applied electrical current that is effectively used for the material removal, excluding losses due to side reactions
Removed mass $m_a(Q)$ [g]	The mass removed from the anode in relation to the current flowing over a specific period of time.

Experimental setup. The removal experiments were performed applying a frontal removal, where the electrode surfaces had the same diameter ($A_{Cathode} = A_{Anode} = 12$ mm). A lateral flushing concept was chosen. The experiments were carried out on a commercially available PEM 800 S ECM machine tool from PEMTec SNC. Fig. 4 shows the machine tool and the removal device.

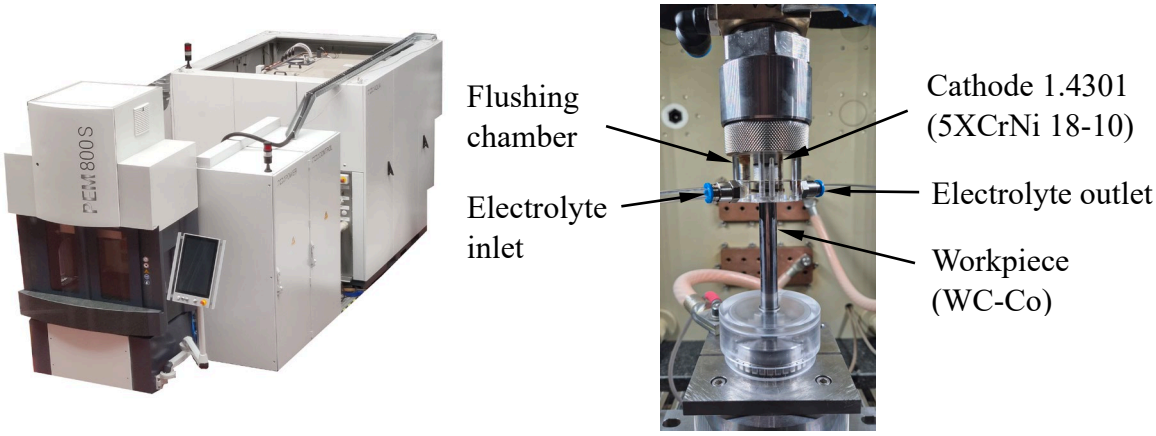

Fig. 4. Experimental setup; left: PEM 800 S, right: Removal device

Process parameters. The applied process parameters are largely derived from the previous PECM experiments. In [9], various process parameters such as electrical voltage U_q, feed rate v_f, pulse width t_p and pulse/oscillation frequency $f_{p/z}$ were varied in a total of 70 removal experiments. Based on this, a parameter set was created that enabled material removal from WC-Co. In MPECM, the process input parameters pulse break t_b and number of pulses n_p have to be added. The selection of the MPECM-specific parameters was determined based on preliminary experiments. Table 3 summarize the final parameter set for the performed removal experiments in this study.

Table 3. Experimental parameters

Symbol	Description	Value
Constant parameters		
Z	Oscillation amplitude	100 µm
f_z	Oscillation frequency	50 Hz
$S_{F\text{-}A}$	Initial front working distance	120 µm
U_q	Electrical voltage	10 V
n_p	Number of pulses	100
t_p	Pulse width	0.5 ms
t_b	Pulse break	0.5 ms
f_p	Pulse frequency	50 Hz
Variable parameters		
v_f	Feed rate	0.01 mm/min – 0.06 mm/min
Electrolyte parameters		
w	Mass fraction $NaNO_3$	8 %
-	ph value electrolyte	8 ± 0.5
p_{El}	Electrical conductivity	70 mS/cm ± 2 mS/cm
σ	Electrolyte inlet pressure	350 kPa
T	Electrolyte temperature	20 °C ± 1 °C

Procedure of the experiments. As can be seen from Table 3, the feed rate v_f of the cathode is the variable parameter of this series of experiments. Experiments with higher feed rates > 0.06 mm/min were conducted but led to a premature manual stop of the experiments. Manual termination serves to protect the machine tool and the removal device from damage and is necessary since the formation of the passivating oxide layer prevents reliable short-circuit detection. Furthermore, the machine's internal parameter analysis showed a decreasing electrolyte flow rate as the experiment progressed – indicating a closing working gap. It can be assumed that with this parameter set, an equilibrium between the feed rate v_f and the removal rate v_a will not be established above a certain feed rate v_f.

The current efficiency η is calculated as the quotient of the effectively removed mass m_{eff} and the specific removal mass m_{sp} [13].

$$\eta = \frac{m_{eff}}{m_{sp}} \tag{2}$$

The specific removal mass m_{sp} is defined by the material constants molar mass M, the electrochemical valence z_A and by Faraday's constant F.

$$m_{sp} = \frac{M}{z_A \cdot F} \tag{3}$$

If the material to be machined consists of several alloying elements, the specific removal mass of the alloy $m_{sp\text{-}alloy}$ is calculated according to Eq. 4, taking into account the mass fraction p_i and the respective density ρ_i:

$$m_{sp-alloy} = \frac{1}{F} \cdot \sum_{i=1}^{n} \frac{M_i \cdot \rho_i}{z_i} \tag{4}$$

The effective removal mass m_{eff} of a removal experiment corresponds to the quotient of the removal mass m_a and the amount of flowed charge Q.

$$m_{eff} = \frac{m_a}{Q} \tag{5}$$

The removal mass m_a can be determined by weighing the workpiece before and after the removal experiment. For direct current processing, the amount of charge flowing Q during material removal is calculated by integrating the process current between the start time t_0 and end time t_1 of a multiple pulse.

$$Q = \int_{t_0}^{t_1} I(t)dt \tag{6}$$

As can be seen from Table 3, the feed rate v_f is the variable parameter for the removal experiments. The removal rate v_f was varied from 0.01 mm/min to 0.06 mm/min in 0.01 mm/min steps to describe the material-specific removal parameters. First, the initial weight of all specimens was weighed using a precision balance Radwag XA 210.4Y PLUS. The removal experiments were carried out at the respective feed rate until a constant current flow was established. After completion of the removal experiments, the surfaces of the specimens were photographed and the final weight weighed. Subsequently, the samples were separated to a defined length for microstructure analysis using wire electrical discharge machining (WEDM), cleaned in an ultrasonic bath, and the surface was analyzed accordingly using SEM.

Results

Surface appearance. Fig. 5 presents the machined test specimens after the experiments.

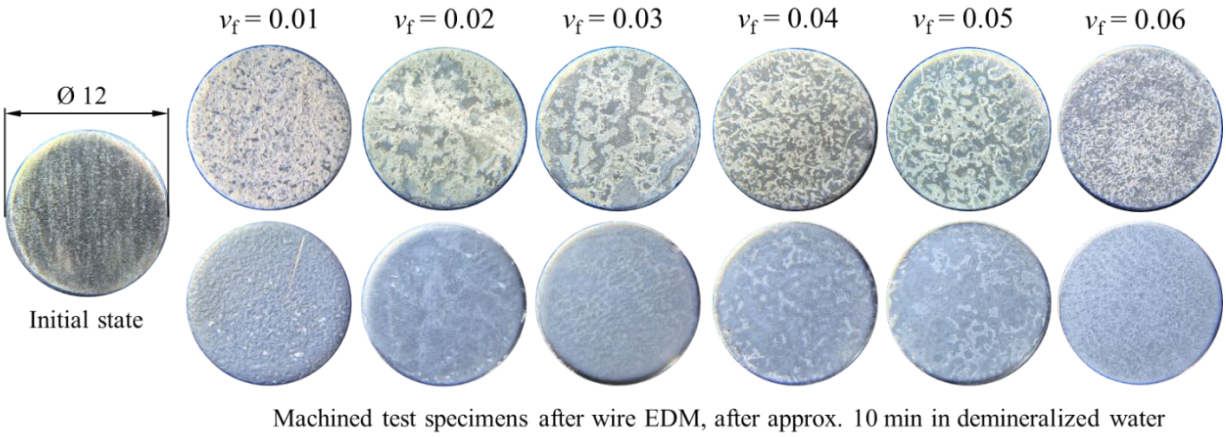

Fig. 5. Initial state surface and resulting surfaces (top view of the test specimen)

The top row shows the state of the machined surfaces immediately after the experiments. The formation of an oxide layer is visible on all surfaces. A firmer, homogeneously distributed oxide layer, compared to the other test specimens, can be seen on the surface machined with the lowest feed rate. The resulting oxide layer becomes less dense with increasing feed rate, but is nevertheless distributed evenly over the entire surface. The bottom row shows the surface of the test specimens after machined by WEDM. It can be seen that the oxide layer has largely flaked off. The surfaces

shown were created solely by resting of the specimens in demineralized water for approximately 10-minutes during the WEDM process.

Removal characteristics. Fig. 6 shows the feed rate v_f of the cathode and the removal rate v_a of the workpiece as a function of the effective current density J for the MPECM parameter set shown in Table 3.

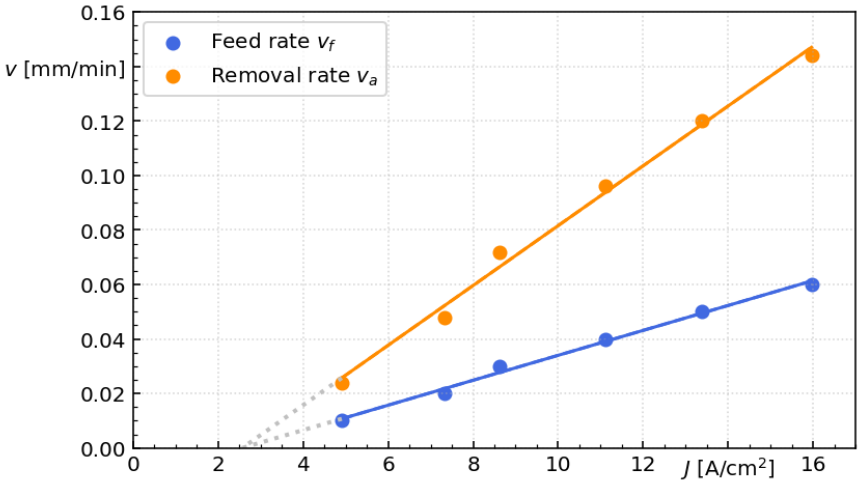

Fig. 6. Resulting feed rate v_f and removal rate v_a as a function of the current density J

Each dot represents a removal experiment. It can be seen that the feed rate v_f and removal rate v_a increase linearly with increasing current density J. Due to the pulse processing, the functions differ in their slope. The existing correlation between the removal rate v_a in z-direction and the current density can be described by a linear correlation function according to Eq. 7 [13].

$$v_a(J) = V_m \cdot J + v_0 \tag{7}$$

The parameter V_m describes the removal volume of WC-Co CKi®12 in a $NaNO_3$ solution with direct current processing. The range of current density J from 5 A/cm² to 16 A/cm² results in removal volume $V_m = 0.0011$ (mm/min)/(A/cm²). The interpolated intersection of the x-axis of the linear function represents the theoretical starting point of material removal and corresponds to a minimum current density of $J_{min} = 2.57$ A/cm². The parameter v_0 describes the intersection point with the ordinate axis. For this removal function, this intersection lies in the negative range. A negative v_0 therefore indicates a transpassive material removal, as a minimum current density can be determined. Table 4 summarizes the parameters.

Table 4. Parameters of correlation function for the removal rate $v_a(J)$

Parameter	J	V_m	v_0	Correlation coefficient R^2
Unit	A/cm²	(mm/min)/(A/cm²)	mm/min	-
Value	5 - 16	0.0011	-0.0028	0.993

Removal mass and current efficiency. The specific removal mass m_{sp} was determined by Faraday's law of electrolysis and describes the mass of the removed material that is theoretically removed by the complete conversion of the electrical charges, provided that the entire electrical charge is fully utilized for the removal. Accordingly, the specific removal m_{sp} [g/C] mass can be used to derive a theoretical removal mass $m_{a\text{-theoretical}}$ [g] [9]. The specific removal mass for the material WC-Co with a proportion of chemical elements according to Table 1 and calculated according to Eq. 4 is $m_{sp} = 281$ µg/C.

Fig. 7 shows a comparison of the calculated theoretical removal mass $m_{a\text{-theoretical}}$ with the removal mass per electrical charge flow Q in the MPECM $m_{a\text{-MPECM}}$ and PECM $m_{a\text{-PECM}}$ [9] experiments.

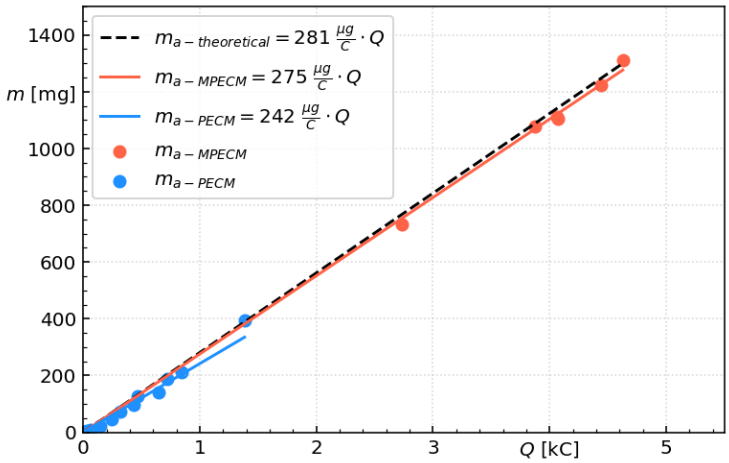

Fig. 7. Calculated and experimental removal mass m_a for the PECM and MPECM process as a function of flowed electrical charge Q

The red and blue dots represent the respective values of the difference weighing. The maximum measurement deviation of the differential weighing's was ± 0.044 mg. In both experimental variants, an increase in the removal weight is visible with increasing electrically flowed charge Q. It can also be seen that slightly more mass per flowed charge was removed in the MPECM removal experiments compared to the PECM removal experiments. While the MPECM experiments showed a stable electrolyte flow rate, the flow rate decreased in the PECM experiments, which, as already mentioned in the sub-chapter "Procedure of the experiments", indicates a closing working gap. Based on the experiments, it can be assumed that processing with MPECM enables a more stable removal process of the WC-Co material. Furthermore, it is noticeable that the slope of the MPECM function is almost identical to the calculated mass removal function $m_{a\text{-theoretical}}$. Since, according to Eq. 4, $m_{a\text{-theoretical}}$ corresponds to a current efficiency η of 100 %, the MPECM experiment series with the selected parameter set has an average current efficiency of 97 % (PECM = 86 % [9]). In the next step, the current efficiency η was examined via the current density J. Fig. 8 shows the course of the current efficiency η as a function of the current density J for the MPECM experiments.

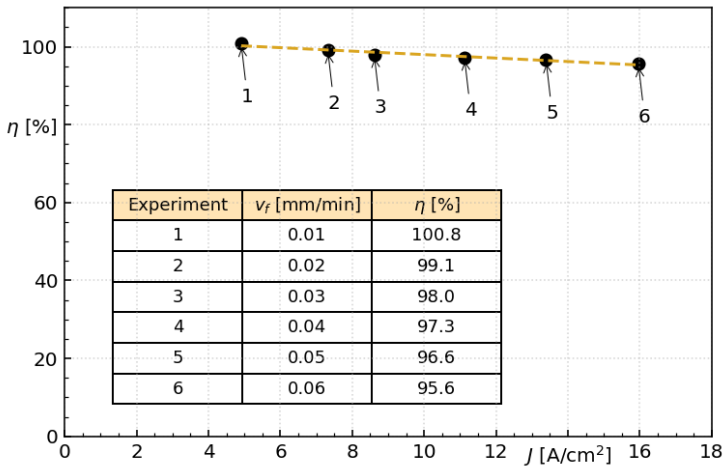

Experiment	v_f [mm/min]	η [%]
1	0.01	100.8
2	0.02	99.1
3	0.03	98.0
4	0.04	97.3
5	0.05	96.6
6	0.06	95.6

Fig. 8. Current efficiency η as a function of current density J for different feed rates v_f

Based on Eq. 2, the current efficiency can be determined from the differential weighing measurements. Current efficiencies exceeding 100 % are possible if the effectively m_{eff} removed mass is greater than that calculated m_{sp} based on Faraday's law. This can be explained by the erosion of tungsten carbides and oxides, which are not electrochemically dissolved in the ECM process but are detected by the weight loss measurement of the specimen [14]. As the feed rate v_f increases, the

current density J increases and the current efficiency η decreases. It appears that at higher current densities, more electrical charge is consumed in side reactions such as the oxidation of the material.

Microstructure. Fig. 9 shows surfaces of tests specimens after the MPECM and PECM experiments.

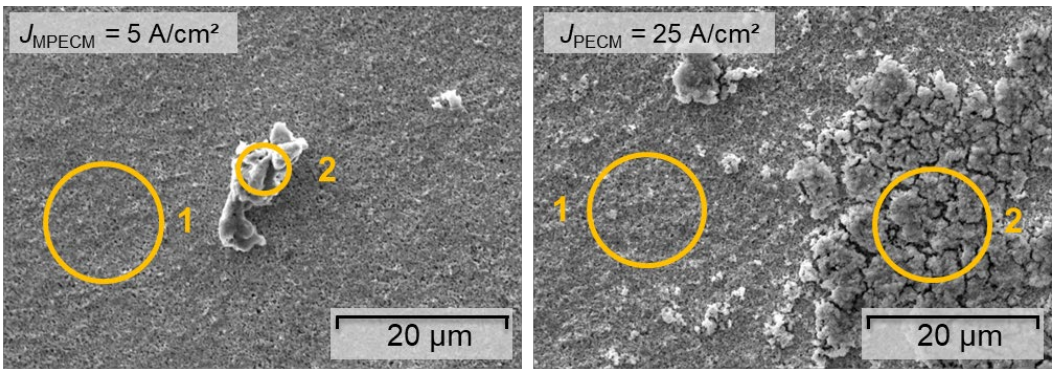

Fig. 9. Topographic SEM images of a cleaned surface after machining, left: MPECM, right: PECM [9]

After ultrasonic bath cleaning, the surface exhibits a homogeneous structure (marked area 1) with oxide particles (marked area 2). Compared to the PECM experiments, the surfaces of the test specimens after the MPECM experiments were covered only with small, scattered oxide residues. In contrast, after the PECM experiments, the surfaces were covered with larger areas of oxide. Table 5 shows the distribution of elements in the marked areas.

Table 5. Chemical composition of test sample compared with the base material

Element		W	C	Co	O
Base material CKi®12	p_i [%]	76.98	12.40	10.63	-
Area 1 MPECM	p_i [%]	82.46	13.30	0.44	3.80
Area 1 PECM [9]	p_i [%]	82.56	11.92	0.72	4.80
Area 2 MPECM	p_i [%]	52.52	28.28	1.44	18.76
Area 2 PECM [9]	p_i [%]	66.02	11.24	4	18.74

EDX analysis of the machined surfaces shows significant removal of the binder metal cobalt for both process variants. The formation of an oxide layer is corroborated by the EDX analysis, which shows a significantly increased oxygen signal in the corresponding areas. These findings are consistent with the reaction described in Eq. 1 and suggest that the formed oxide present in the image can be identified as tungsten trioxide (WO_3). The causes of the observed carbon enrichment and its distribution are subjects of further investigations.

Conclusion

In this study, the electrochemical removal characteristics of WC-Co was analyzed applying the MPECM process with a commercially available ECM machine tool. A neutral sodium nitrate solution was applied as the electrolyte. Based on the results, it can be concluded that the general removal mechanism in the multiple pulse process does not differ from that in the PECM process. An anodic dissolution of the cobalt content and an oxidation of the tungsten content is followed by a mechanical separation of the tungsten oxide layer by electrolyte flow conditions, gas bubbles or cavitation effects. This results in a removal process that, with the selected parameter set, only runs stably at low cathode feed rates. If a certain feed rate is exceeded, the working gap becomes too small, and removal and byproducts, including the tungsten oxide layer, can no longer be reliably flushed out. The consequence is a decreasing flow rate and, corresponding to the increasing gap resistance, a decreasing process flow and an unstable process. Nevertheless, it has been shown that the short pulse-pause sequence with a resting cathode of the MPECM process stabilizes the aforementioned removal

mechanism in comparison to the sinusoidal processing of the PECM process. For future experiments, the integration of ultrasound into the PECM and MPECM processes is being intended in order to suppress the formation of the passivating oxide layer.

Acknowledgements

This project is funded by the Federal Ministry for Economic Affairs and Climate Action, following a decision of the German Bundestag. The machine tool PEM 800 S is funded by the German Research Foundation (DFG) with project number 467011871.

References

[1] G.S Upadhyaya, Materials science of cemented carbides — an overview, Mater. Des. 22 (2001) 483-489. https://doi.org/10.1016/S0261-3069(01)00007-3

[2] K. Zeng, X. Wu, F. Jiang, J. Shen, L. Zhu, L. Li, A comprehensive review on the cutting and abrasive machining of cemented carbide materials, J. Manuf. Process 108 (2023) 335-358. https://doi.org/10.1016/j.jmapro.2023.10.042

[3] M. Painuly, R.P. Singh, R. Trehan, Electrochemical machining and allied processes: a comprehensive review. J Solid State Electrochem. 27 (2023) 3189-3256. https://doi.org/10.1007/s10008-023-05610-x

[4] N. Schubert, M. Schneider, A. Michaelis, Electrochemical Machining of cemented carbides, International Journal of Refractory Metals and Hard Materials 47 (2014) 54-60. https://doi.org/10.1016/j.ijrmhm.2014.06.010

[5] X. Qi, X. Fang, D. Zhu, Investigation of electrochemical micromachining of tungsten microtools, IJRMHM 71 (2018) 307-314. https://doi.org/10.1016/j.ijrmhm.2017.11.045

[6] RJ. Leese, A. Ivanov, Electrochemical micromachining: An introduction, Adv. Mech. Eng. 8 (2016). https://doi.org/10.1177/1687814015626860

[7] N. Schubert, Untersuchungen zum Electrochemical Machining von Wolframcarbid-Cobalt, Publication series competencies in ceramics 60 (2021), ISBN 978-3-8396-1689-5

[8] M. Anik, T. Cansizoğlu, S. Çevik, Diffusion Effect on the Anodic Reactions of Tungsten, Turk. J. Chem. 28 (4) (2004) 425-440. https://journals.tubitak.gov.tr/chem/vol28/iss4/4/

[9] A. Thielecke, P. Clauß, R. Petermann, G. Meichsner, P. Damm, L. Berg, G. Jungblut, M. Schäfer, M. Hackert-Oschätzchen, Experimental investigation of electrochemical precision machining process for tungsten carbide-cobalt applying sodium nitrate electrolyte, Procedia CIRP 137 (2025) 368-373. https://doi.org/10.1016/j.procir.2025.06.007

[10] A.Schubert, G.Meichsner, M.Hackert-Oschätzchen, A.Martin, J.Edelmann, Precision and Micro ECM with Localized Anodic Dissolution, ICIT&MPT 8 (2011). ISBN 978-961-6692-02-1

[11] R. Petermann, P. Clauß, G. Meichsner, J. Vogel, M. Hackert-Oschätzchen, Method for the Characterisation of the Material Removal in Modulated Pulsed Electrochemical Machining, Procedia CIRP 137 (2025) 134-139. https://doi.org/10.1016/j.procir.2025.01.110

[12] DIN SPEC 91399, Method for determining process input parameters for precision electrochemical machining – requirements, criteria, definitions, DIN Media GmbH (2018). https://dx.doi.org/10.31030/3007935

[13] G. Meichsner, M. Hackert-Oschätzchen, M. Krönert, J. Edelmann, A. Schubert, M. Putz, Fast Determination of the Material Removal Characteristics in Pulsed Electrochemical Machining, Procedia CIRP 46 (2016) 123-126. https://doi.org/10.1016/j.procir.2016.03.175

[14] T. Haisch, E. Mittemeijer, J.W. Schultze, Electrochemical machining of the steel 100Cr6 in aqueous NaCl and $NaNO_3$ solutions: microstructure of surface films formed by carbides, Electrochim. Acta 47 (2001) 235-241. https://doi.org/10.1016/S0013-4686(01)00561-8